

Multi-pathogen situational assessment and forecasting of respiratory disease in Aotearoa New Zealand

Michael J. Plank^{1,2}, Alys R. Young^{3,4}, Katharine L. Senior^{3,5}, Ruarai J. Tobin^{3,6}, Mitchell O’Hara-Wild⁷, Fiona Callaghan⁸, Freya Shearer^{3,5}, and Oliver Eales^{3,6}

¹School of Mathematics and Statistics, University of Canterbury, Christchurch, New Zealand

²Te Pūnaha Matatini, Auckland, New Zealand

³Infectious Disease Dynamics Unit, Centre for Epidemiology and Biostatistics, Melbourne School of Population and Global Health, University of Melbourne, Melbourne, Victoria, Australia

⁴College of Science and Engineering, James Cook University, Queensland, Australia

⁵Infectious Disease Ecology and Modelling Team, The Kids Research Institute Australia, Perth, Western Australia, Australia

⁶School of Mathematics and Statistics, University of Melbourne, Melbourne, Victoria, Australia

⁷Monash University, Melbourne, Victoria, Australia

⁸Public Health Agency, Manatū Hauora Ministry of Health, Wellington, New Zealand

Abstract

Real-time analysis of epidemic trends and forecasts can help support public health planning and the response to seasonal respiratory disease. Here, we present two models that were used in a 2025 New Zealand winter situational assessment programme for three respiratory pathogens: SARS-CoV-2, influenza and respiratory syncytial virus (RSV). These models were run weekly from May to October 2025 on real-time disease surveillance data and provided a quantitative representation of the current epidemic trend, along with estimates of the epidemic growth rate and 28-day ahead forecasts of case incidence. Model results and interpretation were provided in weekly reports to public health partners as part of a trans-Tasman winter programme run by the Australia–Aotearoa Consortium for Epidemic Forecasting and Analytics (ACEFA). We compare in-season results that were included in these reports to a retrospective analysis of the complete data for the season. We conclude that real-time analyses performed reasonably well, and identify some areas for improvement in future winter situational assessment programmes.

1 Introduction

Analysis of current epidemic trends and near-term forecasts can contribute to situational awareness and support healthcare capacity planning [1, 2]. This is particularly relevant during the winter respiratory illness season, when healthcare capacity is often stretched [3] due to overlapping respiratory pathogen epidemics. Real-time analysis and forecasting models can help anticipate and plan for increases in hospitalisations or patient load.

Aggregate metrics, such as severe acute respiratory illness, or syndromic surveillance indicators such as influenza-like illness (ILI), are routinely used to monitor the progression of the respiratory illness season. However, these aggregate metrics can mask trends in the composite pathogens that contribute to the aggregate metric [4]. For example, a decreasing trend in an aggregate metric could mask a growing epidemic of a single composite pathogen, and therefore lead to underestimation of future healthcare demand. Quantifying pathogen-specific trends (or strain-specific trends where relevant) provides richer and more valuable information than looking at trends in aggregate metrics alone [5].

Real-time trend analysis and forecasts have been applied to a variety of pathogens including influenza [6, 7], dengue [8], Zika [9], Ebola [10], diphtheria [11]. They can also play an important role in pandemic response by adding an early warning dimension to pandemic respiratory surveillance, and were used extensively during the COVID-19 pandemic [12–15].

In this paper, we describe a winter situational assessment programme for respiratory diseases, which was implemented for the first time in New Zealand in 2025. This programme was run by the Australia–Aotearoa Consortium for Epidemic Forecasting and Analytics (ACEFA) that oversees a trans-Tasman situational assessment programme, including the Australia–Aotearoa Forecasting Hub[16]. This hub reflects the structure and activities of other infectious disease forecasting hubs around the world[8].

Our analysis focuses on two important components of situational assessment: real-time epidemic trend analysis and short-term forecasting. We present two separate models, developed by two independent teams, one for trend analysis and one for forecasting. Both of these models were applied to the same surveillance data streams representing SARS-CoV-2, influenza and respiratory syncytial virus (RSV) activity in New Zealand. Our trend analysis model uses Bayesian P-splines [17] to model a case or hospitalisation incidence time series as a smooth function of time. This allows us to estimate quantities such as the epidemic growth rate and the effective reproduction number.

Our forecasting model is a latent state model with a renewal process for daily infection incidence [18] and a time-varying reproduction number [19]. The observed variables are daily case notifications and, where available, new daily hospital admissions (each of which is some fraction of infections, observed after a distributed time delay). The model is fitted to data using a particle filter (i.e., sequential Monte Carlo) approach [20].

For both models, we compare in-season results that were used in real-time reporting to public health partners against retrospective analysis of complete data for the 2025 season.

2 Methods

2.1 Data

We obtained two de-identified unit record datasets from Te Whatu Ora Health New Zealand. The first dataset contained all reported cases of SARS-CoV-2 in New Zealand since 26 February 2020, including admission date for patients admitted to hospital for treatment for COVID-19. The second dataset contained all patients admitted to hospital in the Auckland and Counties Manukau Regions (Kidz First, Starship, Middlemore and Auckland City hospitals) with severe acute respiratory infection (SARI) who tested positive for either influenza or RSV since 2 January 2025. These data were collected by Public Health and Forensic Science as part of New Zealand’s hospital-based SARI surveillance system [21, 22].

Weekly updates to each dataset were provided throughout the 2025 winter season (15 rounds). For any given dataset, we refer to the latest date on which data were available as the origin date. The final update was received on 23 October 2025 and contained data up to 10 October 2025. From each update of the unit record data, we calculated the daily total recorded number of laboratory-confirmed: SARS-CoV-2 case notifications, new SARS-CoV-2 hospital admissions, new influenza hospital admissions, and new RSV hospital admission.

2.2 Model for trend analysis

We used a Bayesian P-spline model to quantify the past and current trends in two time series: i) SARS-CoV-2 case incidence and ii) SARS-CoV-2, influenza, and RSV hospitalisation incidence. The model has been described in full elsewhere [5]. In brief, we model the logarithm of the expected value of a time series (i.e., cases and hospitalisations) as a smooth function of time, $s(t)$, using a penalised spline. A penalised-spline is a linear combination of N basis splines of degree n , $B_{i,n}(t)$:

$$s(t) = \sum_i^N b_i B_{i,n}(t). \quad (1)$$

where b_i are the basis spline coefficients. For any time series we define a system of third-order basis splines over regularly spaced knots. We set adjacent knots five days apart — this has previously been shown to be a fine enough temporal resolution to capture dynamical effects of SARS-CoV-2 infection prevalence time series data[23]. The system of basis splines extends three knots either side of the time series to prevent edge effects. We assume a second-order random-walk prior on the basis spline coefficients:

$$b_i = 2b_{i-1} - b_{i-2} + u_i, \quad (2)$$

where

$$u_i \sim N(0, \tau^2). \quad (3)$$

This prior penalises changes in the first derivative of the smoothed function (i.e., changes to the growth rate), with the degree of penalisation set by the additional parameter τ . We assume that time series data, $C(t)$, is negative binomially distributed:

$$C(t) \sim \text{NegBin}(e^{s(t)}, k), \quad (4)$$

with an additional parameter k setting the over-dispersion of the data.

We fit the model using a No-U-Turns Sampler (NUTS) [24] implemented in RStan [25]. When fitting the model to the SARS-CoV-2 case and hospitalisation time series, we assume uninformative constant prior distributions for the parameters τ and k . When fitting the model to influenza and RSV hospitalisation time series, we assume an informative normally distributed prior distribution for both τ and k with mean and standard deviation taken as the mean and standard deviation of the posterior distributions of the model fit to SARS-CoV-2 hospitalisations (for the same week of reporting). This was done to allow the model to converge, when fitting to the shorter influenza and RSV time series. The Bayesian P-spline model was fit to the previous three years of data (up to the last day of data) for SARS-CoV-2 cases and hospitalisations. The model was fit to the entire continuous time series for influenza and RSV hospitalisations (first day of available continuous data was 2 January 2025). When fitting the model to SARS-CoV-2 case time series we additionally account for day-of-the-week effects in the time series (see [5]).

2.3 Forecasting model

For the forecasting model, we assume that the time-dependent reproduction number, R_t , follows a zero-mean Gaussian process in log-transformed space:

$$\ln(R_t) \sim GP(0, s_n, k(t, t')) \quad (5)$$

where $k(t, t')$ is the covariance function which we assume to be the Matern 5/2 function:

$$k(t, t') = \frac{s_0^2 2^{1-\nu}}{\Gamma(\nu)} \left(\frac{\sqrt{2\nu}|t-t'|}{l} \right)^\nu K_\nu \left(\frac{\sqrt{2\nu}|t-t'|}{l} \right) \quad (6)$$

where $\nu = 5/2$, s_0 is the signal standard deviation, l is the correlation time scale, and K_ν is the modified Bessel function of the second kind and order ν . To implement the Gaussian process model, the value of $\ln(R_t)$ is drawn conditional on the known values of $\ln(R_s)$ for $s = 0, \dots, t-1$ using the method described in [26], with observation noise standard deviation s_n .

We assume the number of new daily infections I_t on day t follows the Poisson renewal process:

$$I_t \sim \text{Pois} \left(R_t \sum_{s=1}^{m_g} g_s I_{t-s} \right) \quad (7)$$

where g_s is the probability mass function for the generation interval ($s = 1, \dots, m_g$) and m_g is the maximum generation interval.

The expected number of infections with a report date on day t (Z_t) and the expected number of infections with a hospital admission date on day t (H_t) are calculated via forward convolutions:

$$Z_t = \sum_{s=0}^{m_r} u_s I_{t-s} \quad (8)$$

$$H_t = \sum_{s=0}^{m_h} v_s I_{t-s} \quad (9)$$

where u_s and v_s are the probability mass functions of the distribution of time from infection to reporting and time from infection to hospital admission respectively, and m_r and m_h are their maximum values.

We assume that the case-hospitalisation ratio P_t on day t follows a Gaussian random walk in log-transformed space with fixed variance σ_P^2 :

$$\ln(P_{t+1}) \sim N(\ln(P_t), \sigma_P^2) \quad (10)$$

We assume that the observed number of cases, C_t , and new hospital admissions, A_t , on day t are drawn from conditionally independent negative binomial distributions (parameterised by mean and dispersion):

$$C_t \sim \text{NegBin}(p_c \omega_{c,t} Z_t, k_c), \quad (11)$$

$$A_t \sim \text{NegBin}(p_c \omega_{h,t} P_t H_t, k_h), \quad (12)$$

where p_c is the proportion of infections that are reported as cases (assumed to be fixed), and $\omega_{c,t}$ and $\omega_{h,t}$ are day-of-the-week effects for reported cases and hospital admissions, respectively. Note that the latent variables Z_t and H_t include all infections, whereas the observed variables C_t and A_t represent the subset of infections that were reported as cases or hospitalised, respectively. The case ascertainment ratio p_c is non-identifiable from the data, and so we set $p_c = 1$. This means that the latent variable I_t represents the daily incidence of new infections that will eventually be reported as cases.

Eqs. (11)–(12) define a likelihood function for a given observed value of C_t in terms of $\omega_{c,t} Z_t$ and for a given observed value of A_t in terms of $\omega_{h,t} P_t H_t$. Note that the model includes the flexibility to specify either or both of these distributions as a Poisson distribution by setting the relevant dispersion parameter $k = \infty$.

We estimate the day-of-the-week effects, $\omega_{c,t}$ and $\omega_{h,t}$, directly from the data via

$$\omega_{*,t} = \frac{7 \sum_{s=t \bmod 7} \tilde{X}_s}{\sum_t \tilde{X}_t} \quad (13)$$

where \tilde{X}_t is the relevant observed quantity (either reported cases for $\omega_{c,t}$ or hospital admissions for $\omega_{h,t}$) on day t . The summations are taken over an integer number of weeks leading up to the origin date, up to a maximum of 16 weeks depending on how much past data is available. This assumes that the day-of-the-week effects are constant over this time period.

For details of the initialisation and fitting method, see Supplementary Material Sec. S1. Parameter values used in the model are shown in Table 1 (for further details, see Supplementary Material Sec. S1.3).

We evaluated probabilistic forecasts y against subsequently observed data y^{obs} using the continuous ranked probability score (CRPS), defined as

$$\text{CRPS}(y, y^{\text{obs}}) = \int_{-\infty}^{\infty} \left(F(y) - \mathbb{I}(y > y^{\text{obs}}) \right)^2 dy \quad (14)$$

where $F(y)$ is the cumulative distribution function for the forecast and $\mathbb{I}(\cdot)$ denotes the indicator function. CRPS was calculated numerically using $N = 2000$ randomly selected particles. The

Pathogen-specific parameters	SARS-CoV-2	Influenza	RSV
Generation interval	3.3 ± 3.5 days	2.6 ± 1.3 days	7.5 ± 2.1 days
Time from infection to reporting	6.3 ± 3.1 days	-	-
Time from infection to admission	6.3 ± 3.7 days	3.6 ± 2.1 days	6.9 ± 2.7 days
Pathogen-independent parameters			
Maximum generation interval		$m_g = 15$ days	
Maximum time from infection to reporting		$m_r = 25$ days	
Maximum time from infection to admission		$m_h = 25$ days	
Gaussian process signal s.d.		$s_0 = 0.1$	
Gaussian process autocorrelation time scale		$l = 30$ days	
Gaussian process observation noise s.d.		$s_n = 0.001$	
Probability of infection being reported		$p_c = 1$	
Dispersion parameter for observed daily cases		$k_c = 25$	
Dispersion parameter for observed daily admissions		$k_h = 25$	
Coefficient of variation of initial case-hospitalisation ratio		$P_{CV} = 0.025$	
Number of particles		$N = 10^5$	
Fixed resampling lag		$L = 42$ days	

Table 1: Table of model parameter values. Parameters shown as $\mu \pm \sigma$ show the mean (μ) and standard deviation (σ) of the assumed distribution. Note the model nominally assumes $p_c = 1$ (meaning that all modelled infections are eventually reported as cases), but this parameter does not affect model output for observed variables (daily cases and hospital admissions), only for the latent daily infection variable I_t , which we treat as being identifiable only up to multiplication by an unknown case ascertainment ratio, which we assume to be constant.

CRPS was calculated on log-transformed values so that it can be interpreted a measure of relative rather than absolute error in forecast counts [27].

The code used to produce the results in this article is publicly available [28].

3 Results

We begin by summarising the overall epidemic trends of SARS-CoV-2, influenza and RSV as seen retrospectively in the full season’s data (Sec. 3.1). Then we describe the real-time weekly reporting that we carried out throughout the season (Sec. 3.2, and evaluate the performance of trend estimates and forecasts made in real-time against subsequently available data (Sec. 3.3–3.4).

3.1 Overall epidemic trends

SARS-CoV-2 cases began increasing in New Zealand from April 2025 (Figure 1). Cases increased until late-June/early-July when a peak in modelled cases was reached (approximately 28 cases per day). Cases decreased for approximately two weeks before stabilising, following a small resurgence in the epidemic growth rate from mid-July. SARS-CoV-2 cases were then stable until mid-August, before declining until the end of the study period (October). SARS-CoV-2 hospitalisations exhibited broadly similar temporal dynamics to SARS-CoV-2 cases (Figure 2). The rise in SARS-CoV-2 case and hospitalisations coincided with an increase in the proportion of genomically sequenced cases that were due to the NB.1.8.1 lineage, which increased from low levels in early May to around 90% by the end of July [29]. This introduction of a new variant with a transmission advantage over established variants potentially contributed to overall growth in SARS-CoV-2 epidemic activity.

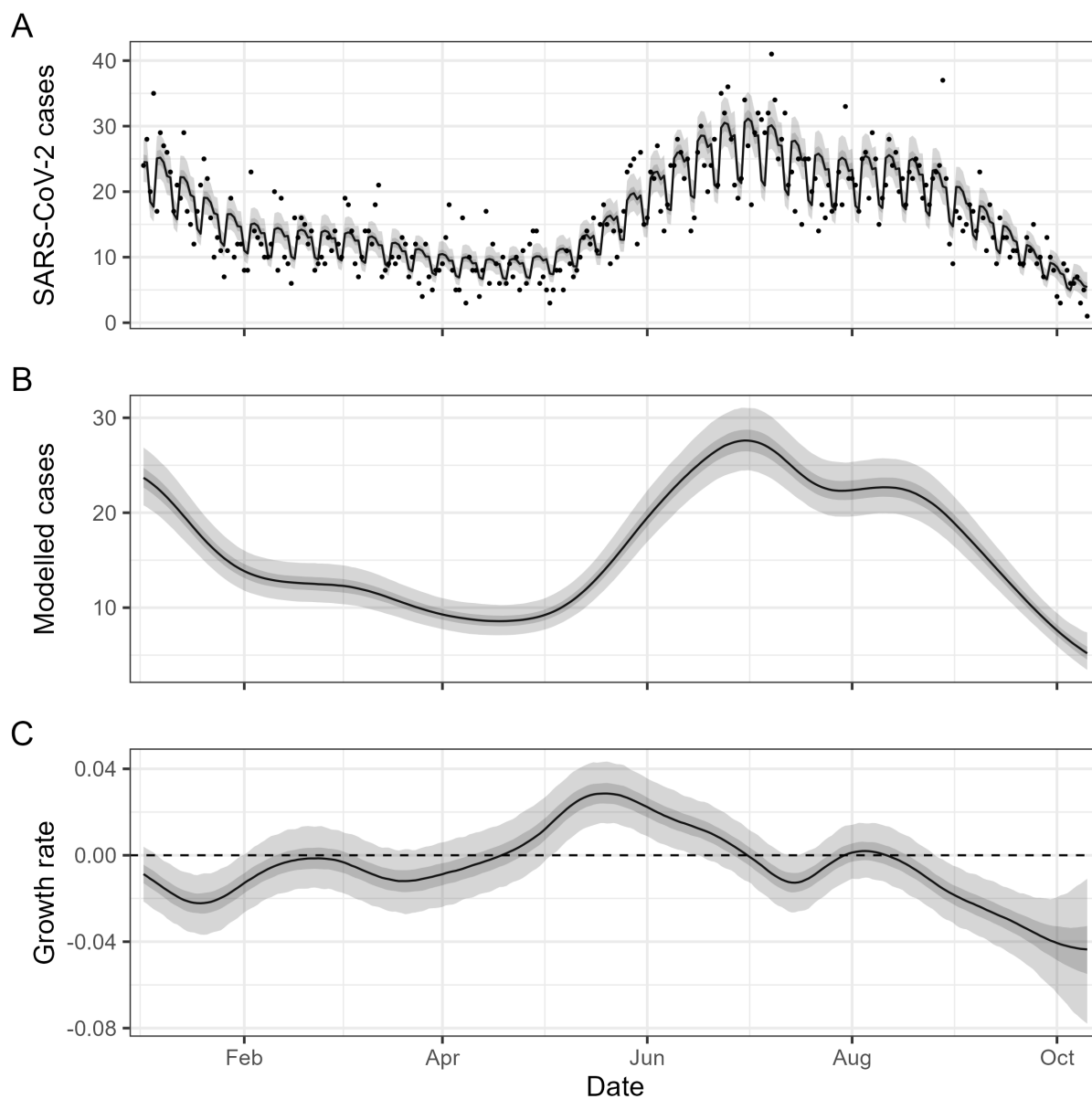


Figure 1: Modelled trends in SARS-CoV-2 cases fitted to full season data. (A) Daily SARS-CoV-2 cases (points) and daily SARS-CoV-2 cases modelled using a Bayesian P-spline model, including a day-of-the-week effect (line and shaded region). (B) Modelled trend in SARS-CoV-2 cases (with day-of-the-week effect removed yet still included in the model). (C) Growth rate inferred from the modelled trend in SARS-CoV-2 cases (with day-of-the-week effect removed). The dashed line indicates a growth rate of zero reflecting the threshold between epidemic growth or decline. For all panels we include the model posterior distribution's median (line) and 50% and 95% credible intervals (dark shaded and light shaded regions).

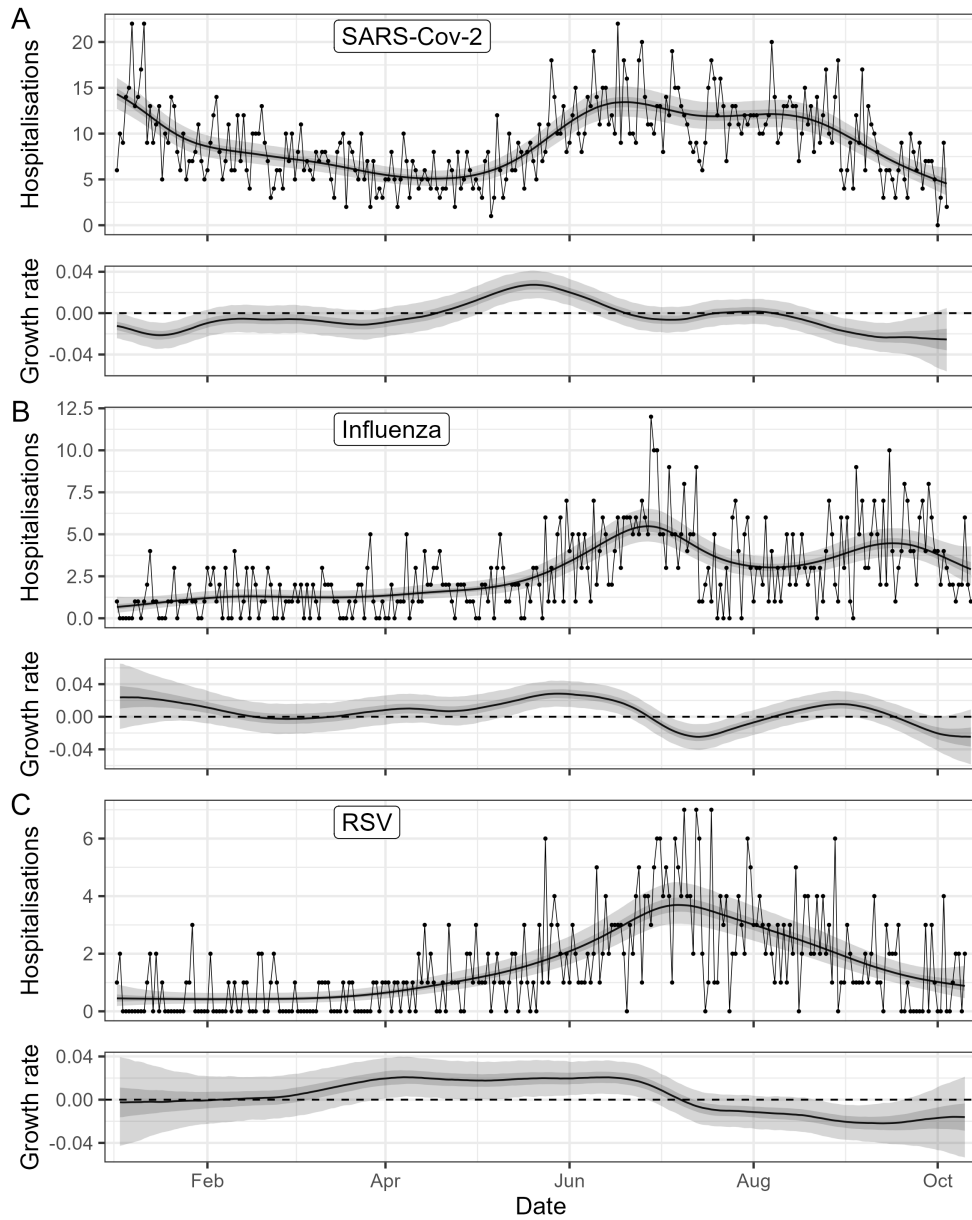


Figure 2: Modelled trends in hospitalisations fitted to full season data for: (A) SARS-CoV-2; (B) influenza; and (C) RSV. In the top panel for each pathogen we plot the daily number of hospitalisations (points) and modelled trend in hospitalisations (line and shaded regions) using a Bayesian P-spline model that does not include a day-of-the-week effect. In the bottom panel for each pathogen we plot the growth rate inferred from the modelled trend in hospitalisations. The dashed line indicates a growth rate of zero (the threshold between epidemic growth or decline). For all panels we include the model posterior distribution's median (line) and 50% and 95% credible intervals (dark shaded and light shaded regions).

There were two peaks in influenza hospitalisations over the course of the season: one in late-June; and one in mid-September. There was only one peak in RSV hospitalisations, occurring in early-July. It is not clear when the modelled daily number of influenza and RSV hospitalisations began increasing due to the low daily numbers of outcomes in these time series and resulting high level of uncertainty estimated by the statistical smoothing model.

3.2 Real-time reporting

We analysed case and hospitalisation time series in real-time during the 2025 season, producing 15 reports for distribution to the New Zealand Ministry of Health and Te Whatu Ora Health New Zealand from 6 June (Report 1) to 3 October 2025 (Report 15). Each report presented estimates of past and current trends in cases and hospitalisations — including estimates of growth rates, doubling/halving times, and the probability the growth rate was greater than zero (cases/hospitalisations growing) — and, where available, 28-day ahead forecasts. An example report (Report 6, produced on 1 August 2025) is included in Supplementary Material Sec. S3. We chose Report 6 because earlier reports did not include forecasts as these were still undergoing performance evaluation. Due to reporting delays, the results in this report were based on data up to 27 July 2025 for SARS-CoV-2 and 19 July 2025 for influenza and RSV. Forecasts show a 28-day time horizon from these respective origin dates.

3.3 Evaluation of real-time estimates of past and current trends

We compared estimates made in real-time over the course of the season to final end-of-season estimates made with data available after season reporting had finished (final data received 23 October 2025). Real-time estimates of trends in SARS-CoV-2 cases showed good agreement to the end-of-season estimate, with overlapping 95% credible intervals (Figure 3). The largest disagreements between real-time and end-of-season estimates were observed in late-July (reports 5–7), when real-time estimates suggested epidemic activity was decreasing faster than estimated at the end of the season. During this period there was a transient increase in the epidemic growth rate. There were also substantial revisions to the data received in real-time (counts were revised upwards in the following week’s data), which likely biased our real-time estimates downwards.

Real-time estimates of expected SARS-CoV-2 hospitalisations were higher than the end of season estimate for most rounds of reporting (Figure 4). This was likely due to significant revisions to data made over the entire study period (e.g., data available in the first round of reporting was revised multiple times over the study period). RSV and influenza hospitalisation data was far more stable, with fewer revisions made to the data (and data for a single revised at most once). Accordingly, real-time estimates of expected hospitalisations and their trends for influenza and RSV showed greater agreement with end-of-season estimates (compared to SARS-CoV-2). The greatest disagreement was observed close to the peaks in hospitalisations, where real-time estimates suggested epidemic activity was continuing to increase. However, the lower credible intervals of these estimates were still captured within the end-of-season estimates.

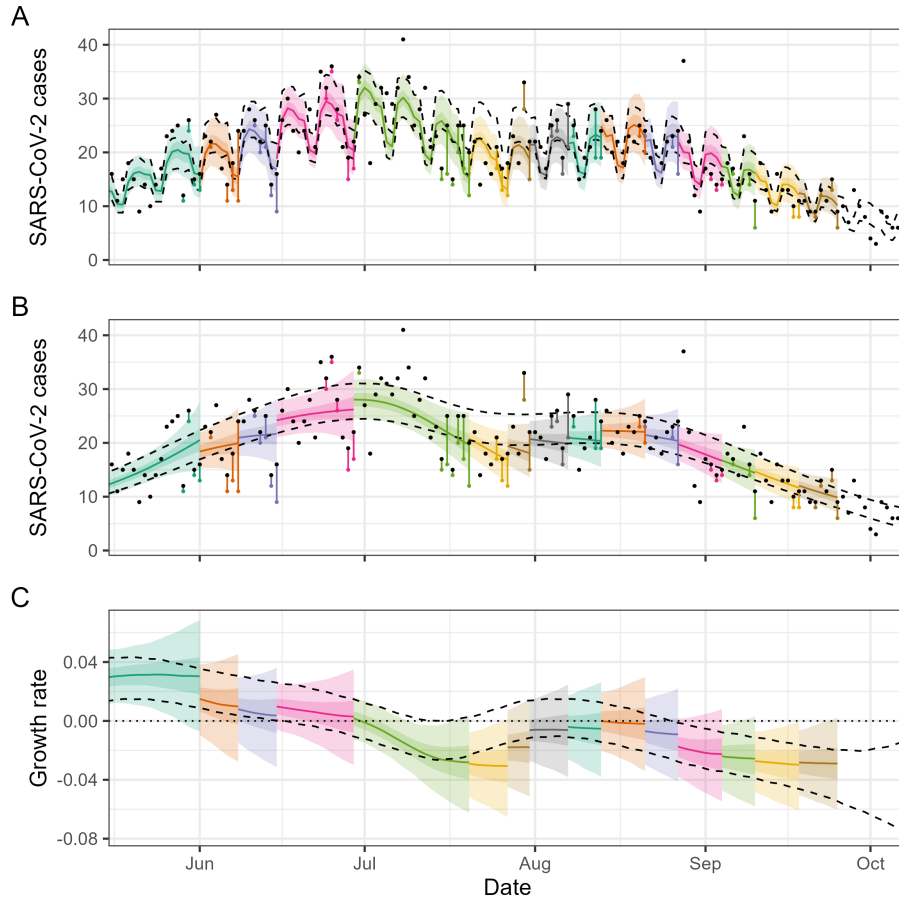


Figure 3: Modelled trends in SARS-CoV-2 cases reported in real-time over the course of the season. (A) Modelled trends in SARS-CoV-2 cases including day-of-the-week effect (lines and shaded region). (B) Modelled trends in SARS-CoV-2 cases with day-of-the-week effect removed (lines and shaded region). (C) Growth rate (lines and shaded region) inferred from the modelled trend in SARS-CoV-2 cases (with day-of-the-week effect removed). For all panels real-time estimates (coloured lines and shaded regions) are compared to 95% credible intervals of end-of-season estimates (black dashed lines). For all real-time estimates (coloured by round), we include the model posterior distribution's median (line) and 50% and 95% credible intervals (dark shaded and light shaded regions). We include the real-time model estimates up to the final day of data (for periods greater than the previous rounds final day of data). In (A) and (B) the daily SARS-CoV-2 cases for the final end-of-season dataset (black points) and the daily SARS-CoV-2 cases in the real-time datasets (points coloured by round) are connected by lines to highlight revisions to data used in real-time analyses. For example, during the fourth round (first pink) there are visible pink data points connected directly to the black end-of-season data; the data in pink is the data available when models were estimated, the data was revised upwards in the following round where it matched the end-of-season data. Note that when coloured points (and connecting lines) can not be seen then there has been no revisions to the data. When a coloured point can be seen and is the same colour as the real-time estimate for the same period (and connected directly to a black data point), it indicates that the number of cases for a specific day was revised (upwards in most instances) in the following round of data, but was not revised in any further rounds of data).

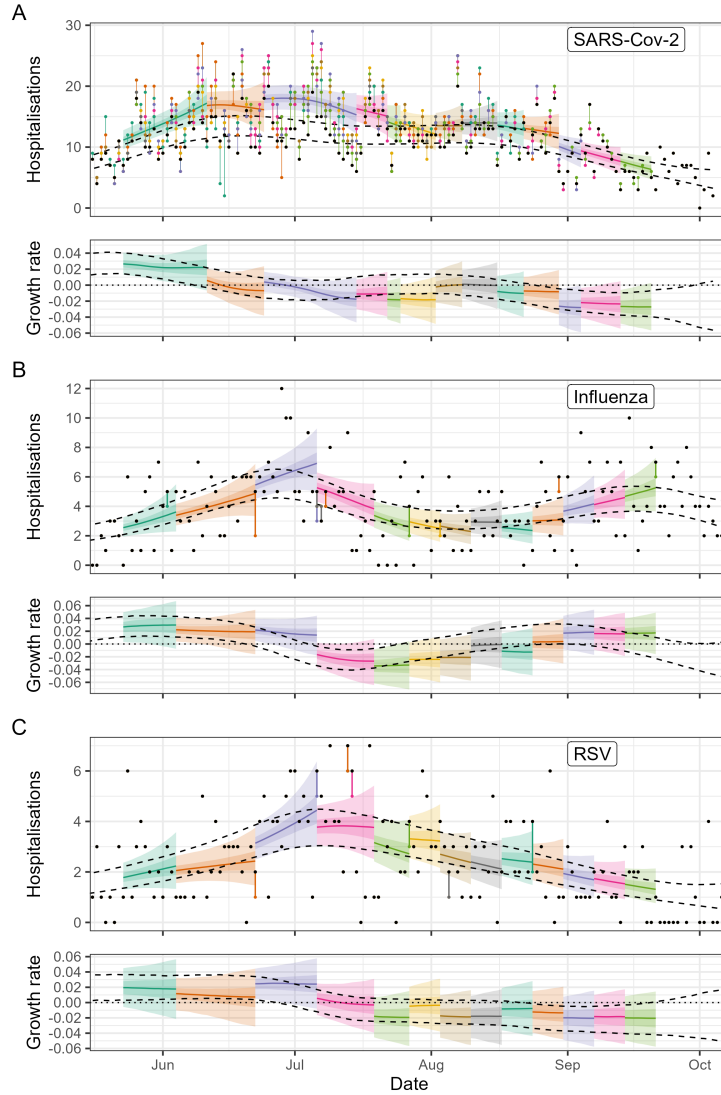


Figure 4: Modelled trends in hospitalisations reported in real-time over the course of the season. Modelled trends in hospitalisations are shown for: (A) SARS-CoV-2; (B) influenza; and (C) RSV. For each pathogen we plot: (top panels) modelled trends in hospitalisations (lines and shaded region); and (bottom panels) growth rate (lines and shaded region) inferred from the modelled trend in hospitalisations. For all panels real-time estimates (coloured lines and shaded regions) are compared to 95% credible intervals of end-of-season estimates (black dashed lines). For all real-time estimates (coloured by round) we include the model posterior distribution’s median (line) and 50% and 95% credible intervals (dark shaded and light shaded regions). We include the real-time model estimates up to the final day of data (for periods greater than the previous rounds final day of data). The daily number of hospitalisation for the final end-of-season dataset (black points) and the daily number of hospitalisations in the real-time datasets (points coloured by round) are connected by lines to highlight revisions to data used in real-time analyses. Note that when coloured points (and connecting lines) can not be seen then there has been no revisions to the data. Note that for SARS-CoV-2 hospitalisations some data were revised in multiple rounds and so many points can be seen for the same time point.

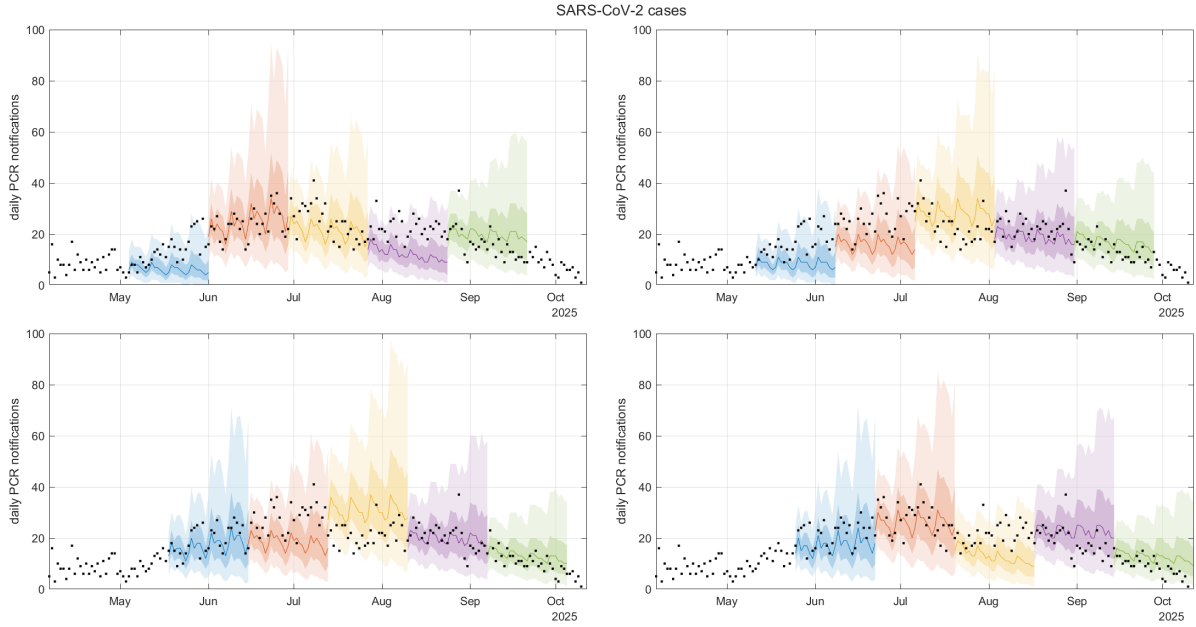


Figure 5: In-season forecasts for daily SARS-CoV-2 cases at different origin dates (coloured lines and bands) alongside subsequently observed data (black points). Each coloured block in each panel shows a forecast generated using a specific origin date, corresponding to the left-hand side of the block (blue – 4 May to 25 May; red – 1 June to 22 June; yellow – 29 June to 20 July; purple – 27 July to 17 August; green – 24 August to 14 September). Each panel shows the same data with forecasts from a different set of origin dates. For each forecast, we show the posterior median (line) and 50% and 90% credible intervals (dark shaded and light shaded regions).

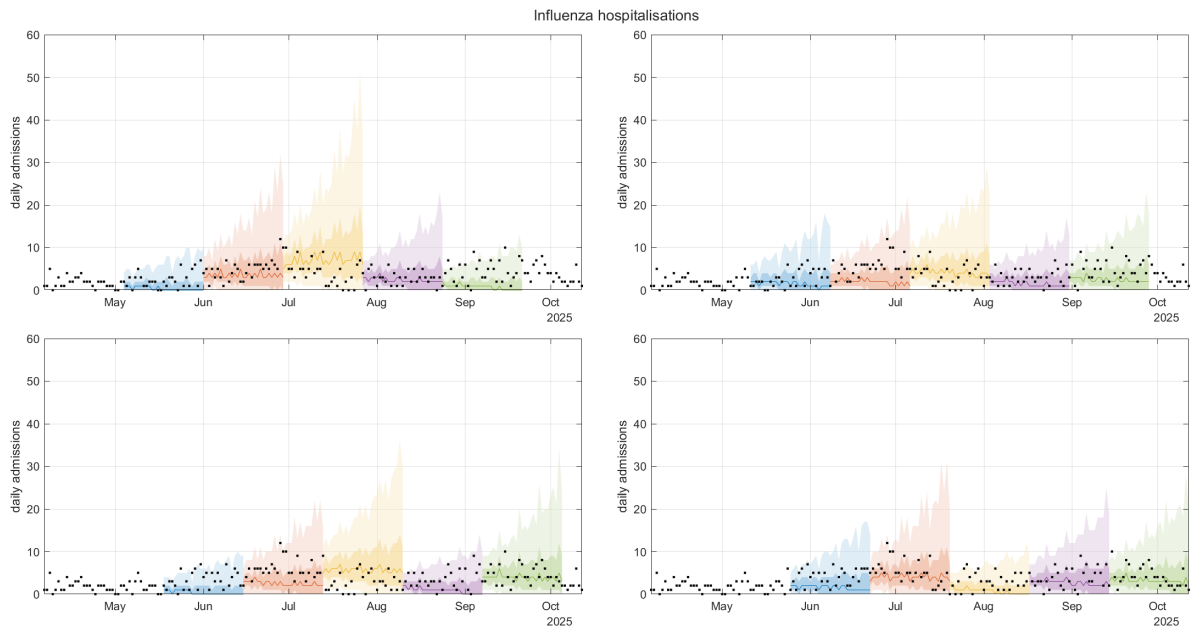


Figure 6: In-season forecasts for daily new influenza hospitalisations at different origin dates (coloured lines and bands) alongside subsequently observed data (black points). Each coloured block in each panel shows a forecast generated using a specific origin date, corresponding to the left-hand side of the block (blue – 4 May to 25 May; red – 1 June to 22 June; yellow – 29 June to 20 July; purple – 27 July to 17 August; green – 24 August to 14 September). Each panel shows the same data with forecasts from a different set of origin dates. For each forecast, we show the posterior median (line) and 50% and 90% credible intervals (dark shaded and light shaded regions).

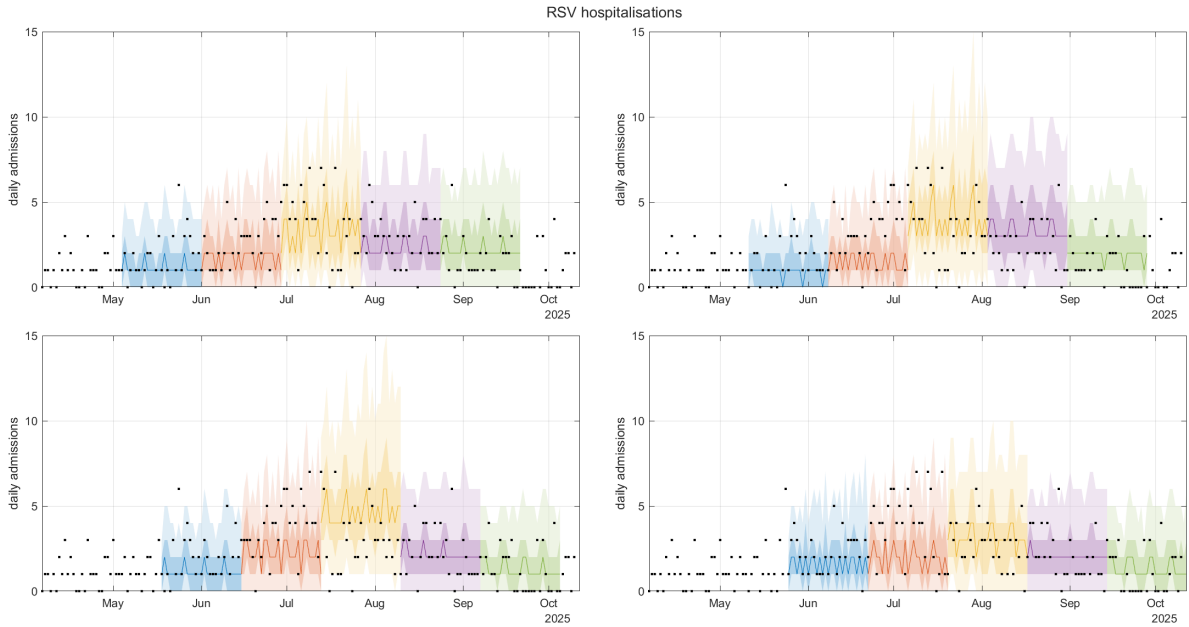


Figure 7: In-season forecasts for daily new RSV hospitalisations at different origin dates (coloured lines and bands) alongside subsequently observed data (black points). Each coloured block in each panel shows a forecast generated using a specific origin date, corresponding to the left-hand side of the block (blue – 4 May to 25 May; red – 1 June to 22 June; yellow – 29 June to 20 July; purple – 27 July to 17 August; green – 24 August to 14 September). Each panel shows the same data with forecasts from a different set of origin dates. For each forecast, we show the posterior median (line) and 50% and 90% credible intervals (dark shaded and light shaded regions).

3.4 Evaluation of real-time 28-day forecasts

To evaluate forecast performance over the season, we compared the forecasts produced for 20 weekly origin dates (from 4 May 2025 to 14 September 2025) against subsequently available data for the whole season (Figures 5–7). In these figures, each coloured block shows a 28-day forecast generated for a specific origin date, corresponding to the left-hand side of the block. Different colours are used to make the distinction between different origin dates clear. For the first two origin dates shown for SARS-CoV-2 cases (red blocks in Figures 5a and b), the forecasts tended to underestimate subsequent data (although this mostly fell within the 95% credible interval). At most subsequent origin dates, the forecasts appeared to capture the data reasonably well. There were some origin dates where the forecast underestimated (e.g., blue block in Figure 5a) or overestimated the data (e.g., green block in Figure 5c), but again the data mostly fell within the 95% credible interval. Trends in the SARS-CoV-2 hospitalisation data and forecast performance (Figure S1) closely mirrored those for SARS-CoV-2 cases.

Influenza forecasts (Figure 6) performed reasonably well throughout the season, although with wider credible intervals (compared to SARS-CoV-2) as a result of the relatively small numbers of influenza hospitalisations in the data. For the 29 June origin date (green block in Figure 6a), which was around the peak in influenza activity, the forecast exhibited very wide credible intervals and somewhat overestimated subsequent data. However, the following week’s forecast (green block in Figure 6b) provided a better prediction of the subsequent trend.

RSV forecasts (Figure 7) performed reasonably well at predicting the trend and the high levels of variability in the data, but were potentially less informative for public health officials due to the wide credible intervals and very small numbers of RSV hospitalisations.

Figure 8 shows the mean CRPS as a function of the forecast time horizon, averaged over all origin dates. The CRPS can be interpreted as a measure of the relative difference between the probabilistic forecast distribution and the subsequent data point, i.e. smaller CRPS indicates better forecast accuracy. Most forecasts showed a trend of increasing mean CRPS with time horizon, indicating that as expected, forecasts tend to be less accurate at longer time horizons. Overall, the forecast for SARS-CoV-2 (Figure 8a, blue) cases had the lowest mean CRPS (between 0.1 and 0.35). The forecast for SARS-CoV-2 hospitalisations (Figure 8a, red) performed had a higher CRPS and showed signs of weekly periodicity with spikes at time horizons of 3, 10, 17 and 24 days. This could be due to a day-of-the-week effect that was not fully captured by the model, or due to historical revision of data primarily occurring on the same day of the week.

4 Discussion

We have presented the methods and results of the 2025 New Zealand winter situational assessment programme for SARS-CoV-2, influenza and RSV. This was the first year of the programme; prior to 2025, New Zealand lacked capacity for real-time model-based situational assessment and forecasting for seasonal respiratory diseases. This programme complements traditional surveillance of respiratory disease [22] by improving our ability to interpret and predict epidemiological trends in real-time.

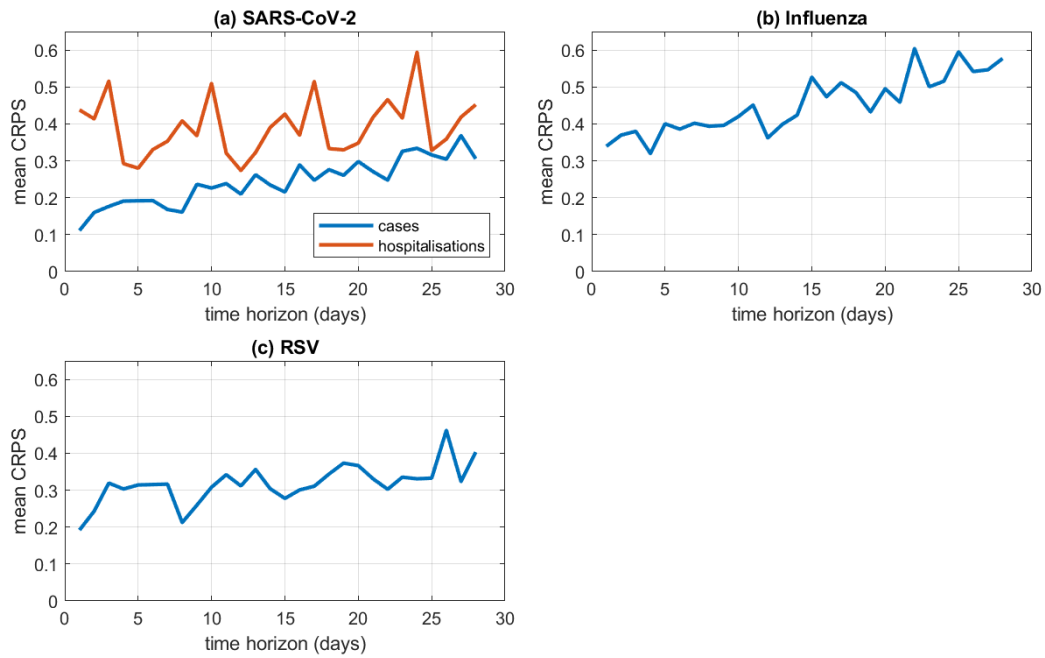


Figure 8: Mean continuous ranked probability scores (CRPS) at different forecast horizons for each of the forecast targets: (a) SARS-CoV-2 cases (blue) and hospitalisations (red); (b) influenza hospitalisations; (c) RSV hospitalisations. CRPS values were calculated on log-transformed data and averaged over all origin dates for a given forecast horizon.

Our forecasts and estimates of current trends performed reasonably well overall, but were worst during periods of rapid change in the epidemic growth rate. This was not a surprising finding. Both models used in our analyses are fundamentally designed to estimate the current trend in the data; the forecast model assumes that this trend continues into the near future, with some gradual reversion to a constant time-series over time. As a consequence, our models cannot predict trends before they start to become apparent in the data. Similarly, our models are likely to be biased when substantial revisions occur to data received in real-time relative to the final data. SARS-CoV-2 cases recorded in the most recent week of data were regularly revised upwards in the following round of data (and influenza and RSV hospitalisations to a lesser extent). This likely biased estimates of current trends and forecasts downwards, but estimates of past trends would have been less affected. In contrast, SARS-CoV-2 hospitalisations were revised frequently, with the same day of data often revised over multiple rounds, biasing estimates of past, current and future trends. This is common because all probable SARS-CoV-2 hospitalisations are initially included in the real-time hospitalisation data. However, hospitalisations may be recoded as diagnoses are updated, and hence SARS-CoV-2 hospitalisations may be retrospectively added or removed. Statistical methods could be developed to quantify revisions in hospitalisation or case counts over time. This would enable these changes to be account for when estimating epidemic trends in real-time, as has been done elsewhere [30].

The timing of peaks in epidemic activity of respiratory pathogens may be indicative of school holiday effects. School holidays ran from 28 June to 13 July 2025. Peaks in SARS-CoV-2 cases and influenza and RSV hospitalisations occurred around this period. School holidays can affect both transmission (by altering contact patterns), as well as testing and healthcare-seeking behaviour, which will influence case and hospitalisation time-series. Without more detailed data on behaviour [31] or underlying infection levels (as opposed to cases) [32], we cannot disentangle the underlying reasons for these changes. It is also possible that similarly-timed peaks would have occurred irrespective of school holidays due to depletion of the susceptible population.

In 2025, an extended influenza season was experienced in southern hemisphere countries, including New Zealand, driven by the emergence of the antigenically distinct subclade K of influenza A/H3N2. Genomic data indicates that this virus was likely seeded into New Zealand from Australia in August 2025 [33], and caused influenza activity to continue into November and December at unusually high levels for the time of year. At the same time, northern hemisphere countries experienced unusually early influenza activity as a result of the same variant [34, 35]. Our results showed an increase in influenza activity in the last few weeks of our analysis. However, most of the subclade K-driven influenza activity in New Zealand occurred after our regular analysis and reporting had ended for the season.

In future seasons, we aim to build on the platform established by this work. Objectives for future work include: expanding the hub approach to include more forecasting models and reporting an ensemble forecast; developing statistical methods to account for revisions to data received in real-time; expanding the types of analysis reported, for example to include age-stratified analysis; and incorporating national data on influenza hospitalisations from the National Minimum Dataset (NMDS) [36].

Data availability statement

The code used to produce the results in this article is publicly available [28]. The raw data cannot be shared publicly for confidentiality reasons, but can be requested from Te Whatu Ora (Health New Zealand) at: data-enquiries@tewhatuora.govt.nz.

Conflict of interest statement

We declare no conflicts of interest.

Ethics statement

This research was carried out under a data sharing agreement between Te Whatu Ora (Health New Zealand) and ACEFA. The terms of this agreement did not require ethics approval for analysis of aggregated data.

Funding statement

MJP was supported by a grant from the Marsden Fund (24-UOC-020) and from Te Niwha Infectious Diseases Research Platform, co-hosted by PHF Science and the University of Otago and provisioned by the Ministry of Business, Innovation and Employment, New Zealand (TN/P/24/UoC/MP). OE was supported by a University of Melbourne McKenzie fellowship. FMS was supported by the National Health and Medical Research Council of Australia through the Investigator Grant Scheme (Emerging Leader Fellowship, 2021/GNT2010051). This research is supported by the Australia–Aotearoa Consortium of Epidemic Forecasting and Analytics (ACEFA), a National Health and Medical Research Council of Australia Centre of Research Excellence (2035303).

Acknowledgements

We are grateful to Te Whatu Ora (Health New Zealand), Manatū Ora (Ministry of Health), and Public Health and Forensic Science for providing weekly data updates throughout the 2025 winter respiratory season and feedback on the content of the weekly reports, in particular Andy Anglemeyer, Harriette Carr, Laura Cleary, Susan Jack, Bex Joslin, Tomasz Kiedrzyński, Zoe Kumbaroff, Andrea McNeill, Natasha Rafter, Imogen Roth, Tanisha Selvaratnam and Fiona Wild. The authors are grateful to Rob Hyndman for feedback on the forecasting model methodology and Alex Kazemi for comments on an earlier version of this manuscript.

References

- [1] Moss R, Fielding JE, Franklin LJ, Stephens N, McVernon J, Dawson P, et al. Epidemic forecasts as a tool for public health: interpretation and (re) calibration. *Australian and New Zealand Journal of Public Health*. 2018;42(1):69-76.

- [2] Lutz CS, Huynh MP, Schroeder M, Anyatonwu S, Dahlgren FS, Danyluk G, et al. Applying infectious disease forecasting to public health: a path forward using influenza forecasting examples. *BMC Public Health*. 2019;19(1):1659.
- [3] Gozzi N, Gioannini C, Milano P, Vismara I, Rossi L, Quaggiotto M, et al. Performance evaluation of RespiCast ensemble forecasts for primary care syndromic indicators of viral respiratory disease in Europe during the 2023/24 winter season. *medRxiv*. 2025:10.1101/2025.10.30.25339155.
- [4] Eales O, McCaw JM, Shearer FM. Biases in routine influenza surveillance indicators used to monitor infection incidence and recommendations for improvement. *Influenza Other Respi Viruses*. 2024 Dec;18(12):e70050.
- [5] Eales O, Windecker SM, McCaw JM, Shearer FM. Inferring temporal trends of multiple pathogens, variants, subtypes or serotypes from routine surveillance data. *Am J Epidemiol*. 2025 Jun:kwaf119.
- [6] Yang W, Cowling BJ, Lau EH, Shaman J. Forecasting influenza epidemics in Hong Kong. *PLoS Computational Biology*. 2015;11(7):e1004383.
- [7] Zarebski AE, Dawson P, McCaw JM, Moss R. Model selection for seasonal influenza forecasting. *Infectious Disease Modelling*. 2017;2(1):56-70.
- [8] Reich NG, Lauer SA, Sakrejda K, Iamsirithaworn S, Hinjoy S, Suangtho P, et al. Challenges in real-time prediction of infectious disease: a case study of dengue in Thailand. *PLoS Neglected Tropical Diseases*. 2016;10(6):e0004761.
- [9] Chowell G, Hincapie-Palacio D, Ospina J, Pell B, Tariq A, Dahal S, et al. Using phenomenological models to characterize transmissibility and forecast patterns and final burden of Zika epidemics. *PLoS Currents*. 2016;8:ecurrents-outbreaks.
- [10] Funk S, Camacho A, Kucharski AJ, Lowe R, Eggo RM, Edmunds WJ. Assessing the performance of real-time epidemic forecasts: A case study of Ebola in the Western Area region of Sierra Leone, 2014-15. *PLoS computational biology*. 2019;15(2):e1006785.
- [11] Finger F, Funk S, White K, Siddiqui MR, Edmunds WJ, Kucharski AJ. Real-time analysis of the diphtheria outbreak in forcibly displaced Myanmar nationals in Bangladesh. *BMC Medicine*. 2019;17(1):58.
- [12] Cramer EY, Ray EL, Lopez VK, Bracher J, Brennen A, Castro Rivadeneira AJ, et al. Evaluation of individual and ensemble probabilistic forecasts of COVID-19 mortality in the United States. *Proceedings of the National Academy of Sciences*. 2022;119(15):e2113561119.
- [13] Moss R, Price DJ, Golding N, Dawson P, McVernon J, Hyndman RJ, et al. Forecasting COVID-19 activity in Australia to support pandemic response: May to October 2020. *Scientific Reports*. 2023;13(1):8763.
- [14] Sherratt K, Gruson H, Johnson H, Niehus R, Prasse B, Sandmann F, et al. Predictive performance of multi-model ensemble forecasts of COVID-19 across European nations. *eLife*. 2023;12:e81916.

- [15] Plank MJ, Watson L, Maclaren OJ. Near-term forecasting of Covid-19 cases and hospitalisations in Aotearoa New Zealand. *PLoS Computational Biology*. 2024;20(1):e1011752.
- [16] ACEFA. Australia-Aotearoa Consortium for Epidemic Forecasting and Analytics; 2026. Available from: <https://acefa-epi-analytics.org/>.
- [17] Wood SN. P-splines with derivative based penalties and tensor product smoothing of unevenly distributed data. *Statistics and Computing*. 2017;27(4):985-9.
- [18] Fraser C. Estimating individual and household reproduction numbers in an emerging epidemic. *PLoS One*. 2007;2(8):e758.
- [19] Abbott S, Hellewell J, Thompson RN, Sherratt K, Gibbs HP, Bosse NI, et al. Estimating the time-varying reproduction number of SARS-CoV-2 using national and subnational case counts. *Wellcome Open Research*. 2020;5(112):112.
- [20] Steyn N, Parag KV, Thompson RN, Donnelly CA. A primer on inference and prediction with epidemic renewal models and sequential Monte Carlo. *Statistics in Medicine*. 2025;44:e70204.
- [21] Huang QS, Baker M, McArthur C, Roberts S, Williamson D, Grant C, et al. Implementing hospital-based surveillance for severe acute respiratory infections caused by influenza and other respiratory pathogens in New Zealand. *Western Pacific Surveillance and Response Journal*. 2014;5(2):23.
- [22] Public Health and Forensic Science (previously ESR). 2024 acute respiratory illness surveillance report; 2025. Available from: <https://www.phfscience.nz/media/gj3bkkvp/2024acuterespiratoryillnesssurveillancereport.pdf>.
- [23] Eales O, Ainslie KEC, Walters CE, Wang H, Atchison C, Ashby D, et al. Appropriately smoothing prevalence data to inform estimates of growth rate and reproduction number. *Epidemics*. 2022 Jun;40:100604.
- [24] Hoffman MD, Gelman A. The no-U-turn sampler: Adaptively setting path lengths in Hamiltonian Monte Carlo. *J Mach Learn Res*. 2014;15(47):1593-623.
- [25] Stan Development Team. RStan: the R interface to Stan;. Available from: <https://mc-stan.org/>.
- [26] Rasmussen CE, Williams CKI. *Gaussian processes for machine learning*. Cambridge, MA: MIT Press; 2006.
- [27] Bosse NI, Abbott S, Cori A, Van Leeuwen E, Bracher J, Funk S. Scoring epidemiological forecasts on transformed scales. *PLoS Computational Biology*. 2023;19(8):e1011393.
- [28] Plank MJ, Eales O. Github repository: ACEFA-NZ-winter-SAP-2025; 2026. Available from: <https://github.com/michaelplanknz/ACEFA-NZ-winter-SAP-2025>.
- [29] Public Health and Forensic Science. Covid-19 Genomics Insight Dashboard Report 62; 2025. Available from: <https://www.phfscience.nz/media/i4t1e1xb/phf-science-cgid-report-62.pdf>.

- [30] Johnson KE, Tang ML, Tyszka E, Jones L, Nemcova B, Wolfram D, et al. Baseline nowcasting methods for handling delays in epidemiological data. *Wellcome Open Research*. 2025;10:614.
- [31] Eales O, Teo M, Price DJ, Hao T, Ryan GE, Senior KL, et al. Temporal trends in test-seeking behaviour during the COVID-19 pandemic. *Mathematics in Medical and Life Sciences*. 2025 Dec;2(1).
- [32] Eales O, McCaw JM, Shearer FM. Challenges in the case-based surveillance of infectious diseases. *R Soc Open Sci*. 2024 Aug;11(8):240202.
- [33] Dapat C, Peck H, Jelley L, Diefenbach-Elstob T, Slater T, Hussain S, et al. Extended influenza seasons in Australia and New Zealand in 2025 due to the emergence of influenza A(H3N2) subclade K viruses. *Eurosurveillance*. 2026;30:2500894.
- [34] Hay J, Alahakoon P, Greenshields-Watson A, Kendall M, Ghafari M, Wymant C, et al. Evaluation of the epidemiological outlook of the influenza A/H3N2 clade K in England during the 2025-26 season. *Zenodo pre-print*. 2025;10.5281/zenodo.17704679.
- [35] Fieldhouse R. Japan declares a flu epidemic - what this means for other nations. *Nature*. 2025 Oct.
- [36] Te Whatu Ora Health New Zealand. National Minimum Dataset (hospital events); 2025. Available from: <https://www.tewhatauora.govt.nz/for-health-professionals/data-and-statistics/nz-health-statistics/national-collections-and-surveys/collections/national-minimum-dataset-hospital-events>.
- [37] Watson LM, Plank MJ, Armstrong BA, Chapman JR, Hewitt J, Morris H, et al. Jointly estimating epidemiological dynamics of Covid-19 from case and wastewater data in Aotearoa New Zealand. *Nature Communications Medicine*. 2024;4:143.
- [38] Cori A, Ferguson NM, Fraser C, Cauchemez S. A new framework and software to estimate time-varying reproduction numbers during epidemics. *American Journal of Epidemiology*. 2013;178(9):1505-12.
- [39] ACEFA. Distribution library; 2025. Available from: <https://github.com/acefa-hubs/forecast-hub/tree/main/distributions>.

Multi-pathogen situational assessment and forecasting of respiratory disease in Aotearoa New Zealand: Supplementary Material

S1 Supplementary methods	2
S1.1 Forecasting model initialisation	2
S1.2 Forecasting model fitting method	2
S1.3 Parameter values and delay distributions	3
S2 Supplementary results	4
S3 Example report to public health partners	5

S1 Supplementary methods

S1.1 Forecasting model initialisation

We simulate N realisations of the process (referred to as particles). We define an initialisation period t_{init} corresponding to the largest of m_g , m_r and m_h . The value of R_t on the last day of the initialisation period (i.e. $t = t_{\text{init}}$), is drawn from the stationary distribution of the Gaussian process defined in Eq. (5). In other words, $\ln(R_t)$ is drawn from normal distribution with mean 0 and variance s_n^2 . The value of P_t at $t = t_{\text{init}}$ is drawn from a Gamma distribution with mean \bar{P} and coefficient of variation $P_{CV} = 0.025$. The value of \bar{P} is estimated directly from the data as the ratio of total hospitalisations to total reported cases over the first 21 days of the simulation period.

The number of daily infections I_t on day t during the initialisation period was drawn from an independent Poisson distribution for each particle with mean

$$i_t = \frac{\tilde{C}_{t+\bar{r}}}{p_c}, \quad t = 1, \dots, t_{\text{init}}, \quad (\text{S1})$$

where \tilde{C}_t is the smoothed number of observed cases on day t , calculated directly from the case data as a 7-day centred moving average, and \bar{r} is the mean time from infection to reporting.

Note that the exact method of initialisation for R_t , P_t and I_t does not have a substantial effect on model results after an initial burn-in period. The starting time for the simulation was taken to be 250 days prior to the origin date, or the date of first available data, whichever was later.

S1.2 Forecasting model fitting method

At each time step, the N particles were propagated forwards one day by drawing random variables according to Eqs. (5), (7) and (10). Given the observed data on day t , the likelihood L_i of each particle i was calculated according to Eqs. (11)–(12). Note that for SARS-CoV-2, data were available for both daily cases (C_t) and daily hospitalisations (A_t), and so the likelihood of each particle was calculated as the product of the likelihood for C_t and A_t according to Eqs. (11) and (12) respectively. For influenza and RSV, only data on hospitalisations was available, so the likelihood was calculated using Eq. (12) only, with P_t fixed at 1.

At each time step, particles were sampled with replacement with weights L_i and the process was repeated until the final data point (i.e., the origin date) was reached. To avoid particle degeneracy, we used fixed-lag resampling (e.g., see [37]), meaning that only the most recent $L = 42$ days of history were resampled. Future trajectories were simulated by propagating the particles forwards from the origin date in the same way, but without any particle resampling. All forecasts were run for 28 days beyond the origin date.

Once we had obtained fitted trajectories for R_t , P_t , I_t , Z_t and H_t , we generated samples for the observed variables C_t and A_t according to Eqs. (11)–(12).

S1.3 Parameter values and delay distributions

The distributions for the generation interval, time from infection to reporting, and time from infection to hospital admission were assumed to be discretised gamma distributions (parameterised by mean and standard deviation – see Table 1).

For each distribution, we truncated the distribution at a specified maximum value and obtained a discretised probability mass function from the continuous Gamma probability density function via the method of [38]. The minimum generation interval was assumed to be 1 day; the minimum delay from infection to either reporting or hospital admission was assumed to be 0 days (although the probability of this occurring was very low).

The mean and variance of the time from infection to reporting were estimated respectively as the sum of the means and variances of the incubation period and the time from symptom onset to reporting. Similarly for the time from infection to hospital admission. This assumes that the incubation period, the time from symptom onset to reporting and the time from reporting to admission are all independent variables.

Values for the mean and standard deviation of the generation interval and the incubation period were taken from the ACEFA distribution library [39]. Values for the mean and standard deviation of the time from symptom onset to reporting and the time from reporting to hospital admission were taken from [15].

S2 Supplementary results

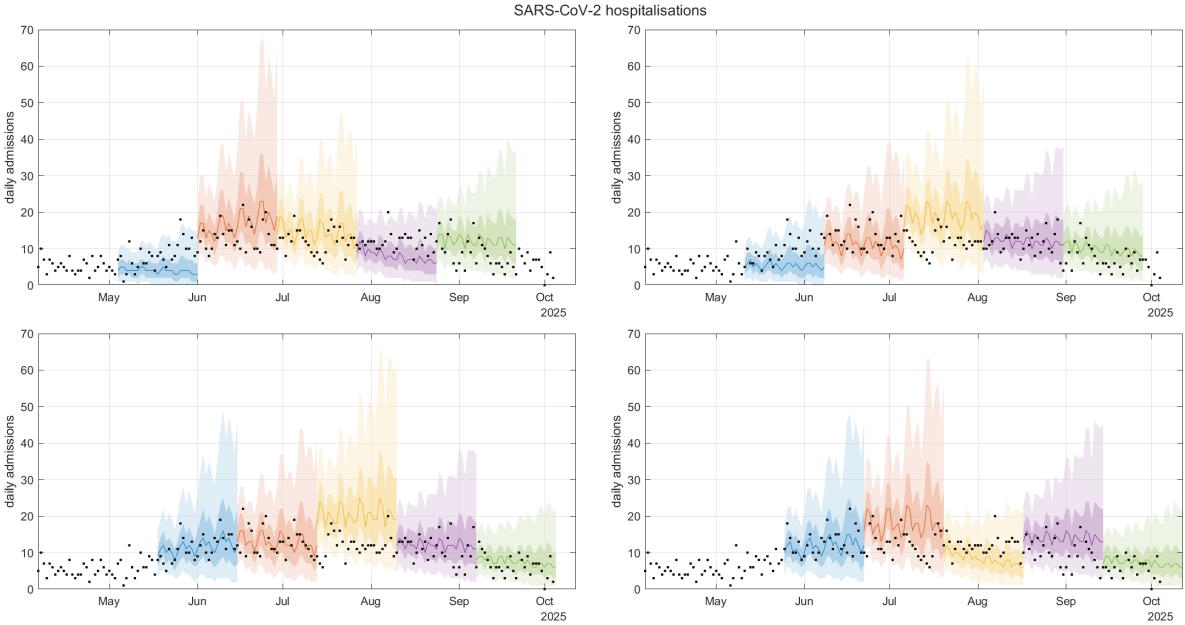


Figure S1: In-season forecasts for daily new SARS-CoV-2 hospitalisations at different origin dates (coloured lines and bands) alongside subsequently observed data (black points). Each coloured block in each panel shows a forecast generated using a specific origin date, corresponding to the left-hand side of the block (blue – 4 May to 25 May; red – 1 June to 22 June; yellow – 29 June to 20 July; purple – 27 July to 17 August; green – 24 August to 14 September). Each panel shows the same data with forecasts from a different set of origin dates. For each forecast, we show the posterior median (line) and 50% and 90% credible intervals (dark shaded and light shaded regions).

S3 Example report to public health partners



ACEFA

AUSTRALIA-AOTEAROA CONSORTIUM FOR EPIDEMIC FORECASTING & ANALYTICS



New Zealand winter respiratory pathogen epidemic analysis

Report no. 6, 2025

1 August 2025



Contributors

ACEFA involves multiple academic research groups from across Australia and New Zealand, including:

- Infectious Disease Dynamics Unit, The University of Melbourne
 - Infectious Disease Ecology and Modelling group, The Kids Institute
 - Defence Science and Technology Group
 - Monash University
 - Infectious Disease Dynamics and Interventions Group, University of New South Wales
 - Infectious Disease Epidemiology and Modelling, Australian National University
 - Infectious Diseases Modelling and Epidemiology Group, University of Queensland
 - Adelaide Data Science Centre, University of Adelaide
 - University of Canterbury
-

Contacts

We welcome any queries, comments, or feedback. Please write to one of our contacts below:

- **Freya Shearer** (Director): freya.shearer@unimelb.edu.au
- **Oliver Eales** (Reporting Lead): oliver.eales@unimelb.edu.au
- **Michael Plank** (Member of Executive Committee): michael.plank@canterbury.ac.nz



Overview

This report was produced on 1 August 2025 for distribution to ACEFA public health partners in New Zealand.

The analysis presented uses data provided by PHF Science and Te Whatu Ora Health New Zealand on 31 July 2025.

We present estimates of current trends in SARS-CoV-2, influenza and RSV epidemic activity, including estimates of the growth rate, effective reproduction number, and doubling/halving times through time up to the last day of data. We also provide 28-day ahead forecasts for PCR-confirmed SARS-CoV-2 cases, SARS-CoV-2 hospitalisations, and SARI hospitalisations for influenza and RSV in the Auckland region. We aim to provide additional analyses and assessment as the season progresses. We are also aiming to consolidate analyses across New Zealand and Australia into a single report to provide a more informative picture across the two countries.

Contents

National picture	4
Appendices	10
References	12



National picture

SARS-CoV-2

- Following an epidemic peak in late-June/early-July, our analysis suggests that **SARS-CoV-2 cases are highly likely to be decreasing**, but stable epidemic activity is also predicted to be possible (Figure NZ-1, NZ-3, NZ-4). On 27 July:
 - Growth rate was estimated to be -0.03 (-0.07 , 0.00) corresponding to a halving time of 23 days (95% CI: halving time of 11 days, doubling time of 600 days).
 - The probability that the growth rate was greater than 0 (cases increasing) was 3%.
 - Effective reproduction number was estimated to be 0.89 (0.79 , 0.99).
 - Four-week ahead forecasts of daily case incidence are uncertain, although consistent with the above trends (Figure NZ-3).
- SARS-CoV-2 hospitalisations have increased since late-April, in line with the increase in cases (Figure NZ-2). Our analysis suggests that **SARS-CoV-2 hospitalisations are most likely decreasing or stable**; trends in hospitalisations will likely continue to follow trends in cases. On 22 July:
 - Growth rate was estimated to be -0.01 (-0.04 , 0.02) corresponding to a halving time of 63 days (95% CI: halving time of 18 days, doubling time of 42 days).
 - The probability that the growth rate was greater than 0 (cases increasing) was 21%.
 - Four-week ahead forecasts of daily hospital admissions are uncertain, although consistent with the above trends (Figure NZ-4).
- In April 2025 modelled case numbers of SARS-CoV-2 were at the lowest levels observed since January 2023 (Figure NZ-1). SARS-CoV-2 case numbers resurged in New Zealand until late-June/early-July and are now expected to be decreasing following an epidemic peak.
 - Similarly timed resurgences and declines have been observed in Australia (not shown). In all Australian states and the Australian Capital Territory there is evidence that SARS-CoV-2 cases are currently decreasing following recent epidemic peaks.
 - Australian Whole Genome Sequencing samples submitted to GISAID show a recent rapid rise in the proportion belonging to lineage NB.1.8.1 (approximately 7% per day growth advantage estimated in NSW for data up to 14 June, and representing ~80% of reported cases) which rose quickly to dominance in Hong Kong over March and April. Rise of new variants is a potential explanation for recent growth in SARS-CoV-2 cases in several jurisdictions.
 - In 2023 and 2024, broadly similar epidemic timings were observed between New Zealand and some Australian jurisdictions (not shown), likely driven by similar population-level immunity profiles and timing of the introduction of new variants. A resurgence (decline) of SARS-CoV-2 cases in one jurisdiction may be predictive of resurgences (declines) in other jurisdictions.

Influenza

- The expected daily number of influenza hospitalisations has increased since late-March. Currently, our analysis suggests that **influenza hospitalisations are likely decreasing**, but stable epidemic activity is also predicted to be possible. There has been a decrease in the growth rate (from well above to well below zero) since mid-June, suggesting that an epidemic peak occurred in late-June/early-July. On 19 July:
 - Growth rate was estimated to be -0.03 (-0.06 , 0.01) corresponding to a halving time of 26 days (95% CI: halving time of 11 days, doubling time of 90 days).
 - The probability that the growth rate was greater than 0 (cases increasing) was 7%.



- Recent school holidays may have contributed to a transient decrease in growth. School holidays may have impacted hospitalisation trends due to either changes in transmission or changes in health-care seeking behaviour, or a combination.
- In Australian jurisdictions sharp decreases in influenza cases in school-aged children were observed coinciding (approximately) with the start of each jurisdiction's school holidays. In some jurisdictions a resurgence in school-aged cases have been observed coinciding with the end of school holidays.
- Four-week ahead forecasts of daily hospital admissions are uncertain, but consistent with the above trends (Figure NZ-4)
- The influenza season in Australia has so far been dominated by influenza A H1N1, which currently represents between 63% (QLD) and 88% (the NT) of all influenza cases. Influenza B activity has also increased across all jurisdictions this season and currently represents between 9% (the NT) and 36% (VIC) of all cases. There has been little influenza A H3N2 activity in Australia this season.

RSV

- The expected daily number of RSV hospitalisations has increased since early-2025 (first day of data). Currently, our analysis suggests that **RSV hospitalisations are most likely stable**, but decreasing or increasing epidemic activity are also predicted to be possible. On 19 July:
 - Growth rate was estimated to be 0.00 (-0.04, 0.03) corresponding to a halving time of 225 days (95% CI: halving time of 18 days, doubling time of 22 days).
 - The probability that the growth rate was greater than 0 (cases increasing) was 43%.
 - Four-week ahead forecasts of daily RSV hospital admissions are uncertain, but consistent with the above trends (Figure NZ-4)
 - In Australia, trends in modelled estimates of RSV cases (not shown) have been broadly similar to the 2023 and 2024 seasons.

Key methodological notes

- We report on epidemic dynamics as inferred from case data or SARI data, noting that these dynamics could reflect changes in the underlying infection dynamics and/or changes in testing and reporting [1].
- Analysis of influenza and RSV activity is based on SARI data from hospitals in the Auckland region only, which may not be representative of national trends.
- All estimates are reported as median (95% credible interval).
- We model dynamics of influenza, RSV and SARS-CoV-2 hospitalisations separately using a single-pathogen Bayesian P-spline model (see Appendix A) that accounts for noise. Note: data on influenza and RSV hospitalisations are PHF Science SARI data from hospitals in the Auckland region; data on SARS-CoV-2 hospitalisations are national COVID-19-related hospital admissions reported to Te Whatu Ora. We do not include the final five days of SARS-CoV-2 data in the hospitalisation analyses to reduce the impact of reporting delays (that would bias our estimates downwards).
- We model dynamics of SARS-CoV-2 cases using a single-pathogen Bayesian P-spline model (see Appendix A) that accounts for day-of-the-week effects and other sources of observation noise.
- We report estimates of the growth rate and effective reproduction number (R_t), noting that R_t estimates are sensitive to the choice of the generation interval distribution [1].

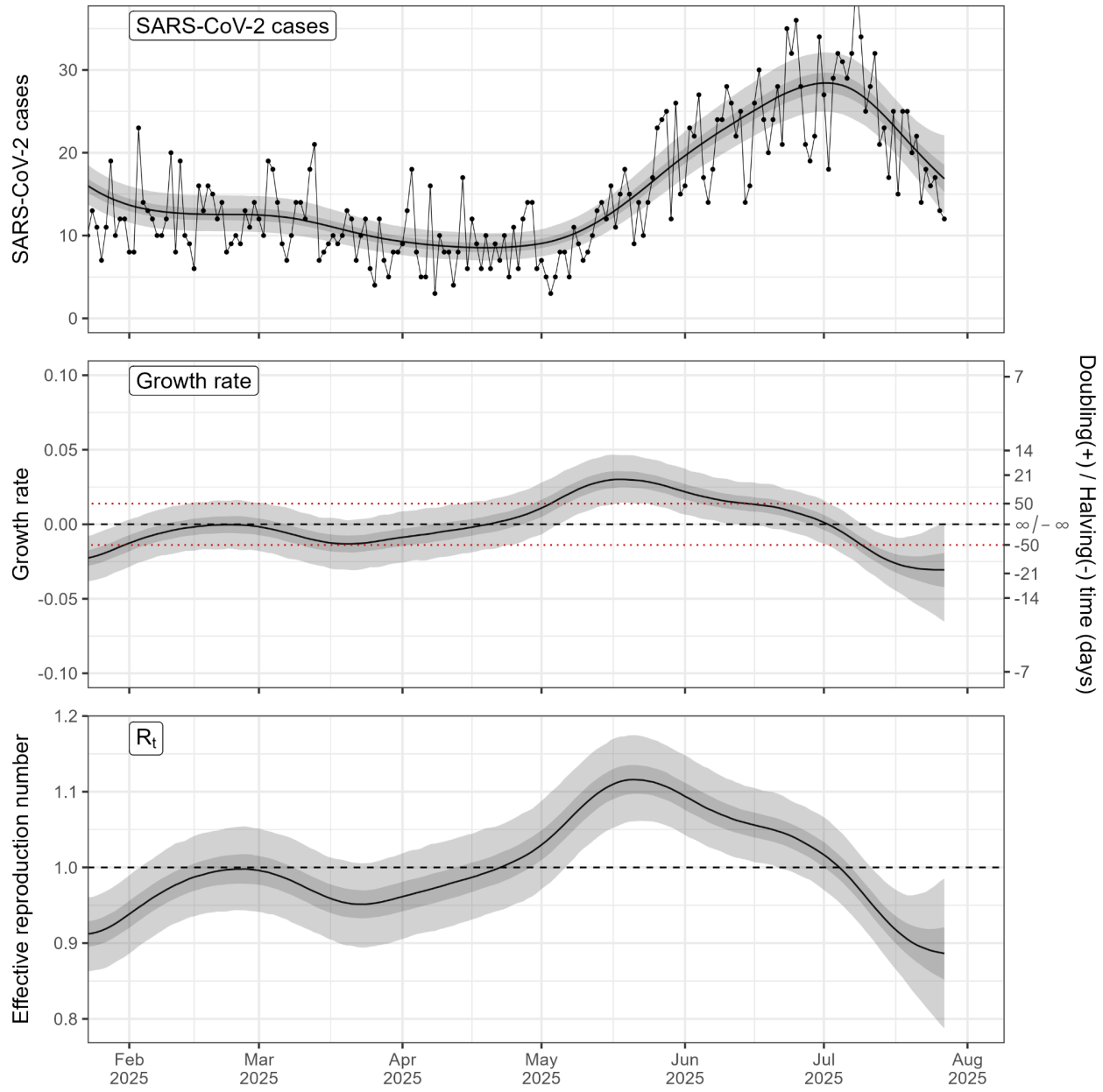


Figure NZ-1: Modelled dynamics of PCR-confirmed SARS-CoV-2 cases in New Zealand. (Top panel) Modelled estimates of the expected number of SARS-CoV-2 cases over time. (Middle panel) Modelled estimates of the daily growth rate in the number of SARS-CoV-2 cases. The dashed black line shows where growth rate equals 0, the transition point between epidemic growth and decline. The right-hand y-axis highlights the corresponding values of the doubling (positive)/halving (negative) time, the time taken for the number of cases to reach double/half its current value. The dashed red lines highlight the region in which the doubling/halving time is greater than 50 days and case numbers are approximately stable. (Bottom panel): Modelled estimates of the effective reproduction number of SARS-CoV-2. The dashed line shows where the effective reproduction number equals 1, the transition point between epidemic growth and decline. All estimates are shown over time with median (line), 50% credible intervals (dark shaded region) and 95% credible intervals (light shaded region).

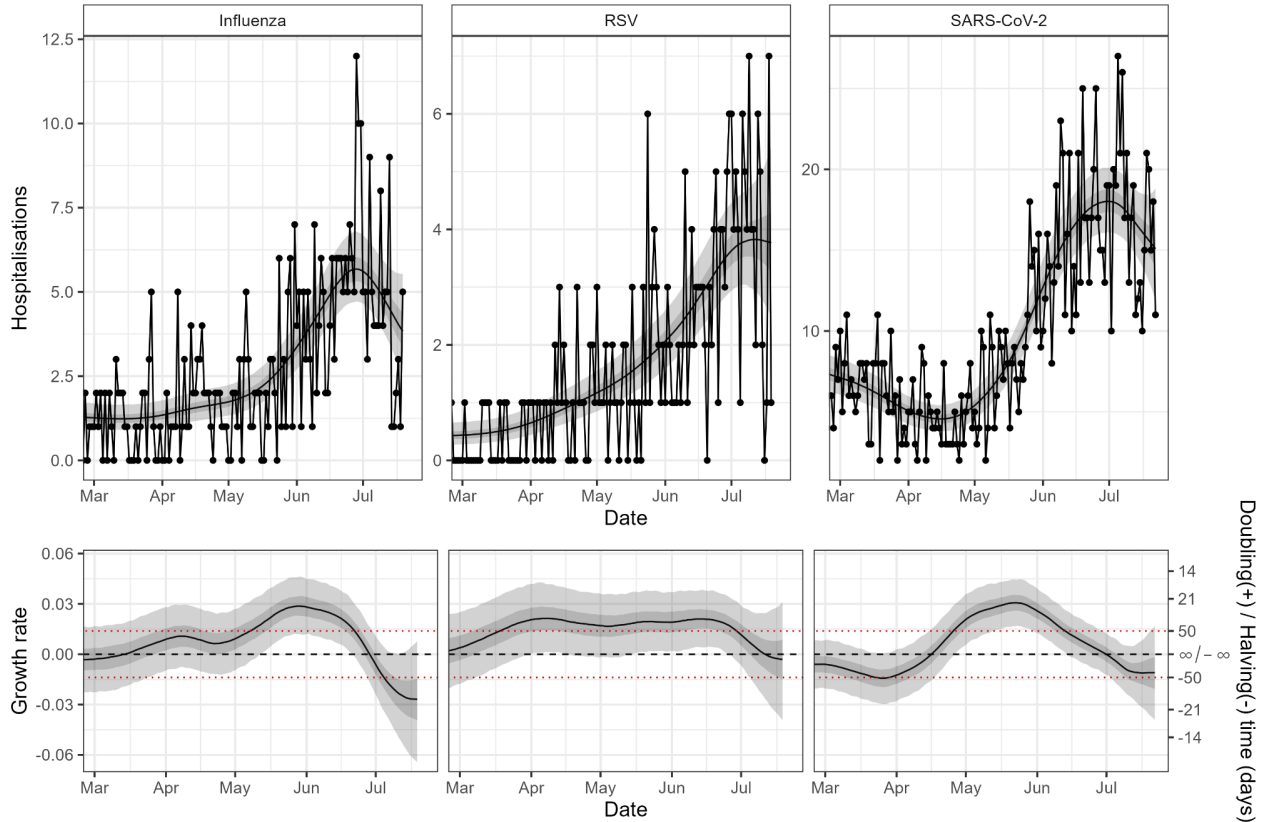


Figure NZ-2: Modelled dynamics of SARS-CoV-2, RSV, and influenza hospitalisations in New Zealand. (Top panels) Modelled estimates of the expected number of hospitalisations over time for each pathogen. Note: data on influenza and RSV hospitalisations are PHF Science SARI data from hospitals in the Auckland region; data on SARS-CoV-2 hospitalisations are national Covid-19-related hospital admissions reported to Te Whatu Ora; these graphs should not be used to make comparisons of the number of hospitalisations between pathogens. (Bottom panels) Modelled estimates of the daily growth rate in the number of hospitalisations for each pathogen. The dashed line shows where growth rate equals 0, the transition point between epidemic growth and decline. The right-hand y-axis highlights the corresponding values of the doubling (positive)/halving (negative) time, the time taken for the number of hospitalisations to reach double/half its current value. The dashed red lines highlight the region in which the doubling/halving time is greater than 50 days and hospitalisation numbers are approximately stable. All estimates are shown over time with median (line), 50% credible intervals (dark shaded region) and 95% credible intervals (light shaded region).

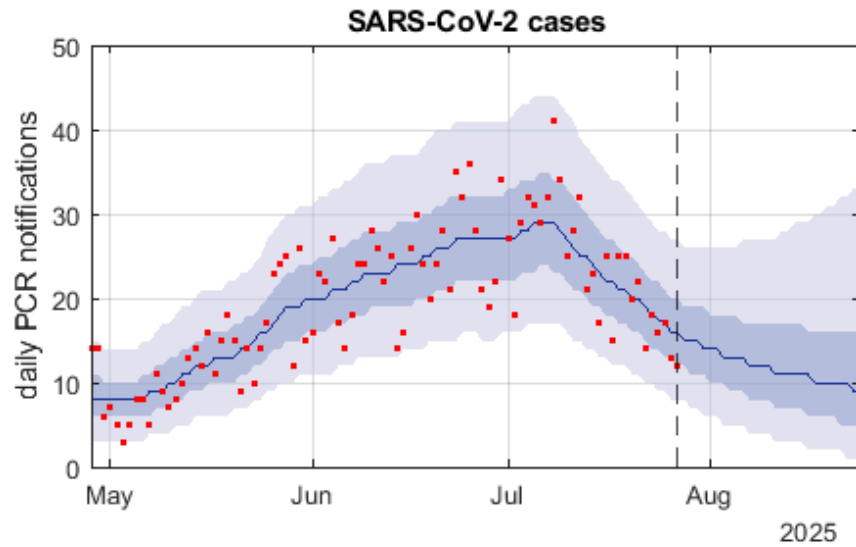


Figure NZ-3: 28-day ahead forecast for PCR-confirmed SARS-CoV-2 cases in New Zealand, showing the median (blue curve), 50% credible interval (dark blue band) and 90% credible interval (light blue band). Observed daily case counts are also plotted (red points). Note that the day-of-week effect in the raw data has been quantified and removed from forecast predictions, and so the most recent data point(s) may not fall within the central forecast quantiles. Forecast based on data up to 27 July 2025.

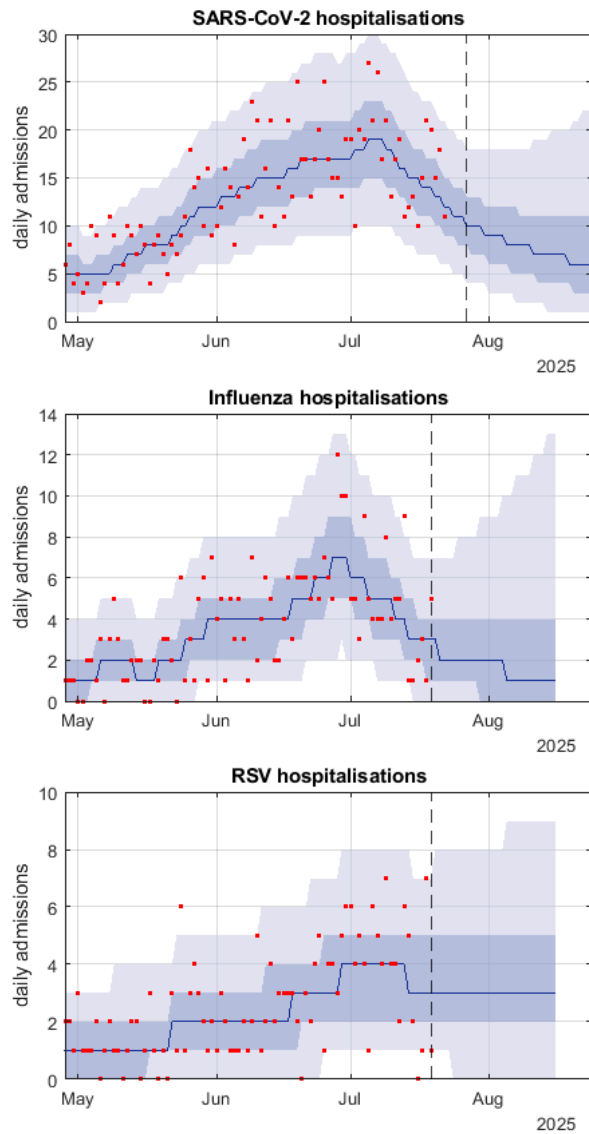


Figure NZ-4: 28-day ahead forecasts of SARS-CoV-2 hospitalisations, influenza SARI hospitalisations, and RSV SARI hospitalisations in New Zealand. Note: data on influenza and RSV hospitalisations are PHF Science SARI data from hospitals in the Auckland region; data on SARS-CoV-2 hospitalisations are national Covid-19-related hospital admissions reported to Te Whatu Ora; these graphs should not be used to make comparisons of the number of hospitalisations between pathogens. For all forecasts we show the median (blue curve), 50% credible interval (dark blue band), 90% credible interval (light blue band) and data (red points) for daily hospital admissions. Forecast based on data up to 27 July 2025 for SARS-CoV-2 and 19 July 2025 for influenza and RSV (indicated by the vertical dashed lines).



Appendix A: Bayesian P-spline models

Single-pathogen Bayesian P-spline model

The single-pathogen Bayesian P-spline model has been described in full in [3]. The model has been extended to account for day of the week effects in the case time series.

The model takes as input an epidemic time-series (e.g., the daily number of cases) and estimates the expected value of the epidemic time-series (i.e., a smoothed trend in the daily number of cases accounting for noise). From the smoothed trend we can then estimate the growth rate and effective reproduction number over time (see below).

Multi-pathogen/multi-variant Bayesian P-spline model

The multi-pathogen/multi-variant Bayesian P-spline model is an extension of the two-variant Bayesian P-spline model described in [4]. The model has also been extended to account for day of the week effects in the case time series.

The model takes as input: (1) an epidemic time-series (e.g., the daily number of cases) and (2) data describing the proportion of tests positive for each pathogen/variant/subtype of interest and the number of negative tests. The model then estimates the expected value of the epidemic time-series (i.e., a smoothed trend in the daily number of cases accounting for noise) for each individual pathogen/variant/subtype. From the smoothed trend for each pathogen/variant/subtype we can estimate their growth rate and effective reproduction number over time (see below). We can also estimate the overall trend in the total epidemic time-series (i.e., the sum of all modelled epidemic time-series)

This model is currently only being used to model the individual dynamics of each influenza type/subtype (influenza A H3N2, influenza A H1N1, and influenza B). If data were available on SARS-CoV-2 lineages and variant groupings of concern (i.e., subset of data describing number of test positive for each variant) then we could also estimate individual dynamics for COVID-19 variants. This would also improve estimates of the overall trend in the total number of SARS-CoV-2 cases.

Estimating the growth rates and doubling/halving times

The growth rate, $r(t)$, of an epidemic time-series (e.g., daily counts of cases) is the difference between the log of the modelled case time-series $C(t)$, across two time points

$$r(t) = \log(C(t)) - \log(C(t - 1)).$$

The doubling/halving time — the time taken for the modelled value of daily cases to double/half — is then given by the equation:

$$\text{doubling or halving time}(t) = \log(2)/r(t).$$

Estimating the effective Reproduction numbers

The effective reproduction number, $R_{eff}(t)$, is the expected number of secondary infections arising from an infected individual. It can be related to the modelled case time-series, $C(t)$, by the equation:



$$R_{eff}(t) = \frac{C(t)}{\int_0^{\infty} c(t-\tau)g(\tau)d\tau},$$

where $g(\tau)$ is the intrinsic generation interval, describing the time distribution between primary and secondary infection. This assumes that the modelled epidemic time-series is a reasonable proxy to infection incidence, in reality the epidemic time-series will likely be lagged and smoother compared to actual infection incidence; this could lead to slightly lagged estimates of $R_{eff}(t)$ that may also be biased when the true value of $R_{eff}(t)$ changes rapidly [5].

For estimates of $R_{eff}(t)$ using the modelled estimates from the Bayesian P-spline we have assumed Gamma distributed generation intervals for SARS-CoV-2, RSV, and all influenza subtypes. The parameters of the Gamma distribution used are:

Pathogen	Shape parameter (gamma distribution)	Rate parameter (gamma distribution)	Mean of distribution	Standard deviation of distribution
SARS-CoV-2 (Omicron) [6]	0.89	0.27	3.30	3.49
RSV [7]	12.76	1.70	7.50	2.10
Influenza (all subtypes) [8]	4.00	1.54	2.60	1.30

Table A1. Generation interval distributions used for estimating reproduction numbers



References

1. Eales O, McCaw JM, Shearer FM. Challenges in the case-based surveillance of infectious diseases. *R Soc Open Sci.* 2024;11: 240202.
2. Eales O, Windecker SM, McCaw JM, Shearer FM. Inferring temporal trends of multiple pathogens, variants, subtypes or serotypes from routine surveillance data. *medRxiv.* 2024. p. 2024.11.03.24316681. doi:10.1101/2024.11.03.24316681
3. Eales O, Ainslie KEC, Walters CE, Wang H, Atchison C, Ashby D, et al. Appropriately smoothing prevalence data to inform estimates of growth rate and reproduction number. *Epidemics.* 2022;40: 100604.
4. Eales O, de Oliveira Martins L, Page AJ, Wang H, Bodinier B, Tang D, et al. Dynamics of competing SARS-CoV-2 variants during the Omicron epidemic in England. *Nat Commun.* 2022;13: 1–11.
5. Eales O, Riley S. Differences between the true reproduction number and the apparent reproduction number of an epidemic time series. *Epidemics.* 2024;46: 100742.
6. Abbott S, Sherratt K, Gerstung M, Funk S. Estimation of the test to test distribution as a proxy for generation interval distribution for the Omicron variant in England. *bioRxiv.* 2022. doi:10.1101/2022.01.08.22268920
7. Perofsky AC, Hansen CL, Burstein R, Boyle S, Prentice R, Marshall C, et al. Impacts of human mobility on the citywide transmission dynamics of 18 respiratory viruses in pre- and post-COVID-19 pandemic years. *Nat Commun.* 2024;15: 4164.
8. Cauchemez Simon, Donnelly Christl A., Reed Carrie, Ghani Azra C., Fraser Christophe, Kent Charlotte K., et al. Household Transmission of 2009 Pandemic Influenza A (H1N1) Virus in the United States. *N Engl J Med.* 361: 2619–2627.